Available online at www.sciencedirect.com

ScienceDirect

www.elsevier.com/locate/jes

JES JOURNAL OF ENVIRONMENTAL SCIENCES

www.jesc.ac.cn

Au nanoring arrays as surface enhanced Raman spectroscopy substrate for chemical component study of individual atmospheric aerosol particle

Hanyun Cheng[1], *Xu Dong*[1], *Yang Yang*[1], *Yiqing Feng*[1], *Tao Wang*[1], *Muhammad Ali Tahir*[1], *Liwu Zhang*[1,2,*], *Hongbo Fu*[1,*]

[1] *Shanghai Key Laboratory of Atmospheric Particle Pollution and Prevention, Department of Environmental Science & Engineering, Fudan University, Shanghai, 200433, China*

[2] *Shanghai Institute of Pollution Control and Ecological Security, Shanghai 200092, China*

ARTICLE INFO

Article history:
Received 29 April 2020
Revised 12 June 2020
Accepted 4 July 2020
Available online 19 July 2020

Keywords:
Raman
SERS
Aerosol
Nanoring
Chemical component

ABSTRACT

Monolayer-ordered gold nanoring arrays were prepared by ion-sputtering method and used as surface enhanced Raman spectroscopy (SERS) substrates to test the individual atmospheric aerosols particle. Compared to other methods used for testing atmospheric aerosols particles, the collection and subsequent detection in our work is performed directly on the gold nanoring SERS substrate without any treatment of the analyte. The SERS performance can be tuned by changing the depth of the gold nanoring cavity as originating from coupling of dipolar modes at the inner and outer surfaces of the nanorings. The electric field exhibits uniform enhancement and polarization in the ordered Au nanoring substrate, which can improve the accuracy for detecting atmospheric aerosol particles. Combined with Raman mapping, the information about chemical composition of individual atmospheric aerosols particle and distribution of specific components can be presented visually. The results show the potential of SERS in enabling improved analysis of aerosol particle chemical composition, mixing state, and other related physicochemical properties.

Introduction

Atmospheric aerosol particles appear in many different forms, such as dust, fumes, smoke, smog and fog, throughout our environment (Andreae and Rosenfeld, 2008). These aerosols affect human health and quality of life through changes in the visibility and toxicity of the atmosphere (Poschl, 2005). Their composition can differ widely depending on their origin (Hallquist et al., 2009). The distribution of particles are influenced by a number of factors including the presence of other aerosols (Virtanen et al., 2010), the chemical equilibrium vapor pressure (Riemer and West, 2013), the internal combustion (Fierce et al., 2016), and so on. The chemistry of aerosols is rich but remains largely unknown due to its complexity and the limitations of the instruments used to investigate it.

Understanding aerosols in detail requires examining the size and chemical composition of the individual particles making up the aerosol (Zhang et al., 2011). The major goal of many aerosol characterization studies would get the detail information of each particle to be traced to its original source (Canagaratna et al., 2007; Noble and Prather, 1996; Roth et al., 2016; Yang et al., 2017). By monitoring the chemical changes occurring in individual particles with high temporal resolution, the chemical dynamics within the aerosol can be unraveled (Xu et al., 2017; Zaveri et al., 2018). Furthermore, analysis at the single-particle level allows immediate detection of atmospheric phenomena, determination

* Corresponding authors.
E-mails: zhanglw@fudan.edu.cn (L. Zhang), fuhb@fudan.edu.cn (H. Fu).

https://doi.org/10.1016/j.jes.2020.07.003
1001-0742/

of exposure levels to harmful industrial aerosols, and detection of chemical warfare agents (Ault and Axson, 2017; Craig et al., 2015). In order to obtain a broad perspective of local, global, and temporal variations of the aerosol phase, some methods for aerosol particle analysis were already reported (Gilardoni et al., 2016; Perrino and Marcovecchio, 2016; Teich et al., 2016). But the limitations of traditional methods (gas chromatography, liquid chromatography, ion chromatography etc.) are the lack of real-time information and an inability to analyze composition on the single particle level. Aerosol particles are most frequently collected by filtration or inertial impaction (Parshintsev and Hyotylainen, 2015). After collecting the compounds of interest, solvent extraction or thermal desorption is used to recover organic compounds from sorbent with subsequent analyses by means of liquid or gas chromatography (Perez-Fernandez et al., 2017). To analyze individual particle size and composition, laser microprobe mass spectrometry (LMMS) and aerosol time-of-flight mass spectrometry (ATOFMS) have proven to be highly efficient methods (Aubriet and Carre, 2010; Elmes and Gasparon, 2017; Hatch et al., 2011; Li et al., 2011). However, using these methods, particles are desorbed or ionized in flight preceding chemical characterization and thus is susceptible to sample deterioration.

During the past decade, surface-enhanced Raman spectrometry (SERS) has been widely used in the characterization and identification of unknown samples in complex chemical environment, and has the advantages of sensitivity and selectivity inherent in the vibrational spectroscopies (Schlucker, 2014). In SERS, the problem of low sensitivity of conventional Raman spectroscopy is circumvented by the enhancement of Raman cross sections by five to six orders of magnitude for molecules adsorbed on metallic surfaces (Cialla et al., 2012). Recently, different research groups have investigated the general usefulness of SERS for the detection of trace amounts of a variety of contaminants, chlorinated pesticides and nicotine (Alharbi et al., 2014; Clauson et al., 2015; Fu et al., 2017; Sun et al., 2019). SERS has been evaluated as a new alternative technique for detection of trace amounts of atmospheric pollutants in aerosols with an inexpensive and straightforward sampling procedure based on collection onto an untreated solid support (filter paper) of aerosols generated from four well established atmospheric pollutants. The detection is performed directly on the filter paper without elution of the analyte, and subsequent analysis by SERS.

The Raman microspectrometry which combines the analysis capabilities of Raman spectroscopy with an optical microscope resolution provides a potential solution for obtaining molecular information on particles of microscopic volume under in situ conditions (Eberhardt et al., 2015). Currently, Raman spectral mapping can be collected by computer-controlled (XYZ) scanning. Moreover, it has also been demonstrated by a number of early investigators that Raman spectrum combined with mapping can be used successfully to study the composition and distribution of atmospheric particles (Ault et al., 2013; Baustian et al., 2012; Offroy et al., 2015). The first use of SERS to detect trace organic and/or inorganic species in ambient atmospheric aerosol particles is presented by Ault et al (Craig et al., 2015). The observations obtained with this method demonstrate the power of SERS to detect inter- and intraparticle variability in ambient secondary organic aerosol particles. In 2017, (Fu et al., 2017) used Klarite as SERS substrate for detecting chemical components of individual aerosol particles, makes it possible to monitor the distribution of organic or inorganic species. Substrates such as Au/Ag nanoparticles are frequently used for SERS study of aerosols, however, they present low measurement reproducibility and low enhancement factor due to the lack of uniformity in the distribution of "hotspots" (Craig et al., 2015). Klarite has high uniformity in the distribution of "hotspots", while the SERS enhancement factor (<6) for aerosols is not satisfying (Fu et al., 2017). We recently reported a Cu/Ag sphere segment void array with EF of tens of times, but fabricating this substrate in large scale is challenging (Dong et al., 2019). It is still a challenge to find a suitable substrate for atmospheric aerosol study. Finding an efficient substrate that have many uniform "hotspots" and can be easily fabricated in large scale is urgently needed for atmospheric aerosol study.

Herein, monolayer-ordered gold nanoring arrays were prepared and used as SERS substrates to test the individual atmospheric aerosols particle for the first time. The SERS substrate was made by depositing gold on the 2D polystyrene sphere (PS) monolayer arrays via an ion-sputtering methods, and then remove the PS by solvent. The thickness and size of nanoring can be easily tuned by changing the sputtering time and the size of PS template. The performance of these nanoring arrays as SERS substrates are evaluated by studying simulated ammonia sulfate aerosol and ambient aerosols.

1. Experimental

1.1. Materials

Polystyrene (PS) nanospheres (diameter 1.0 μm, 5% w/v) was purchased from aladdin®. Ethanol, sodium dodecyl sulfate (SDS), ammonium sulfate ($(NH_4)_2SO_4$, ≥99.0%), sodium sulfate (Na_2SO_4, ≥99.0%), sodium nitrate ($NaNO_3$, ≥99.0%) and tetrahydrofuran (THF, ≥40.0%) were purchased from Sinopharm Chemical Reagent Co., Ltd. All chemicals were used as received unless further mentioned. Deionized water was used in all experiments.

1.2. Self-assembly of 2D colloidal monolayer array of PS particles

The PS nanospheres were sufficiently dispersed in ethanol/water (V/V 1:1) solution by ultrasonic dispersion at a concentration of 5 wt.%. A sodium dodecyl sulfate solution (1%, 20 μL) was added to the water in a tank with the diameter of 12 cm. Then, the PS nanosphere solution was dropped on a flat silica wafer placed, in tilted, at the edge of the tank, and the PS nanospheres slipped onto the surface of water. The PS nanosphere monolayer was then collected onto the fluorine tin oxide (FTO) coated glass slides by lifting. The closely packed PS nanosphere array was obtained on FTO. Finally, these slides with nanosphere array were dried in air.

1.3. Fabrication of ordered gold nanoring arrays

A gold layer was deposited on the 2D PS monolayer arrays coated FTO substrate by an ion-sputtering method. The value is estimated based on the data provided by the instruction manual of the sputter coater (Emitech K550X). In our experiment, the gold layer was obtained at 20 mA for different time duration. Then, the monolayer of close-packed gold nanoshell arrays was lifted by biaxially oriented polypropylene. The PS particles were removed by Tetrahydrofuran, producing a monolayer-ordered gold nanoring arrays adsorbed on the biaxially oriented polypropylene. The nanoring structure was analyzed by Scanning Electron Microscope (SEM; Nova nano SEM 450; FEI, America). The surface morphology and scale was studied using Atomic Force Microscopy (AFM; NANO4; DIGITAL LNSLREIM, America).

1.4. *Aerosol sample collection*

0.1 M solution of ammonium sulfate was used for the laboratory-generated aerosol samples. First, the air flows out of a compressor and into a two-level air filter system (0.1 and 0.01 μm, respectively) to partially remove impurities. Then, the air continues into a two-level air dryer system that can remove nearly 90% percent of the moisture. This is followed by an air filter (0.01 μm) set to prevent the nebulizer from being contaminated by the remaining impurities. The nebulizer generates aerosol droplets with an aerodynamic diameter of 0.5–20 μm, whose median mass aerodynamic diameter range from 1 to 4 μm. Finally, the aerosol droplets are impacted onto substrates using a microanalysis particle sampler. All the samples were collected for 1 min using a homemade microanalysis impactor, operating at a flow rate of 5 lpm. The microanalysis impactor consisted of a mini pump, a flow meter, and a sampling head. After that, we accelerated the dehydration by increasing the temperature to 50°C in an oven. The ambient atmospheric aerosol particles were collected on the roof of the environmental science building at Fudan University in the afternoon of March 14th, 2019. The weather was sunshine with a south breeze. The samples were collected for 6 hr using Anderson 8 grading particle sampler (NVA-800; Staplex, America).

1.5. *Raman measurement*

The gold nanoring substrates and the aerosol particles were probed by using a XploRA confocal spectrometer (Jobin Yvon, Horiba Gr, France). The Raman spectra measurements were recorded using the 532 nm laser excitation and a 100 × Olympus microscope objective lens. The confocal slit width was 100 μm, and exposure time was 5 sec and number of accumulations were 20, detecting a spectral region of 200 to 2000 cm^{-1}. When Raman mapping was acquired, the exposure time was 5 sec and number of accumulations were chosen to be 20.

2. Results and discussion

2.1. *Characterization of Au nanorings*

Fig. 1a is a representative top-view SEM image of the hemispherical concave arrays on the remaining polypropylene after thorough removal of the topmost ordered monolayer PS film, revealing the periodic hexagonal-packed arrangement of geometrical features which is an exact replica of the morphology of the highly ordered PS bottoms. Fig. 1b-f show the top-view SEM images of the sputtered thin Au film on the concave arrays with different sputtering duration (30 sec, 180 sec, 240 sec, 300 sec, 420 sec), demonstrating that the thin Au film is composed of close-packed tiny Au-nanoparticles and uniformly covers the entire surface of the concave arrays. From 30 to 420 sec, as the sputtering duration is prolonged, the average diameter of Au-nanorings is elevated (909±18, 916±27, 924±24, 944±28, 976±34 nm), indicating that the Au-nanorings film were formed gradually. Thus, it is feasible to treat the sputtered Au thin film as dense and continuous Au nanoring arrays. The top-view SEM images of Au nanoring arrays reveals that Au nanorings with different core sizes and shell thicknesses can be fabricated by controlling the sputtering duration. The large area view under Raman microscope (**Fig. S1** in Supporting information) further displays the highly ordered and uniformity of Au nanorings, which is beneficial for the reproducibility of Raman signal.

AFM measurements were used to investigate the fabricated Au nanorings structure in further detail. Fig. 2 shows the AFM images of Au nanoring submonolayer at different sputtering duration of the fabrication process. The line scan and illuminated-top-view images are shown to provide a clearer view of the morphology change. We can find an un-complete but smooth Au shell surface was found when the sputtering duration was 30 sec (Fig. 2a). Next, a complete Au shell was formed by prolong the sputtering duration from 180 to 420 sec and an aperture structure around 400 nm was clearly shown on the top part the Au nanoparticles (Fig. 2b to Fig. 2e), which is close to the observation from SEM images in Fig. 1. Additionally, the top surface of the Au nanoparticles becomes rougher due to the sputtered Au film surface. Fig. 2 indicates the cavity structures in Au nanoparticles. The depth of the cavity is measured from 20 nm to 405 nm, and the inner diameter of the cavity is around 400 nm (Table 1). When the sputtering duration changes from 30 to 180 sec, the inner diameter of the cavity increases from 366 nm to 433 nm, which is due to the accumulation of the Au nanoparticles. From 180 to 240 sec, the size of the aperture structures shrinks largely. We attribute these dimensional deviations of the cavity and the aperture structures to the geometry limit. Afterwards, a larger aperture of 360 nm and 395 nm on the top part of the Au nanoparticles was produced by 300 sec and 420 sec of ion sputtering, respectively. The shell thickness changes with the inner diameter. In addition, a much rougher Au nanoring surface was obtained, which was determined by the applied electrostatic spray deposition during the Au nanoshell preparation process.

2.2. *Characterization of the SERS performance of the Au nanorings*

The prepared Au nanorings were examined as effective SERS substrates for the detection of $(NH_4)_2SO_4$ aerosols, one of typical components in atmospheric aerosol. Fig. 3a displays the SERS spectra of $(NH_4)_2SO_4$ aerosols on the as-prepared Au Nanorings with different sputtering duration. Four distinct bands of SO_4^{2-}, identified as the totally symmetric mode ν_1 at 975 cm^{-1}, the antisymmetric stretching mode ν_3 at 1066 cm^{-1}, the bending modes ν_2 at 451 cm^{-1}, and ν_4 at 612 cm^{-1}, respectively, are clearly observed in the spectrum in Fig. 3, which agree well with the normal Raman spectrum of $(NH_4)_2SO_4$ (Dong et al., 2007). The two peaks at 1445 cm^{-1} and 1700 cm^{-1} results from the contributions of H_2O and NH_4^+ vibrational modes (Dong et al., 2007; Jordanov and Zellner, 2006). In the SERS spectra, it can be seen that the SERS activity of the substrates improves with increase of the Au-sputtering duration from 30 to 420 sec. And the representative peak of $(NH_4)_2SO_4$ was also enhanced by using bare Au nanorings as substrates when the Au-sputtering duration decreases down to 30 sec. The tendency of SERS intensities of the main peak band at 975 cm^{-1} of $(NH_4)_2SO_4$ versus sputtering duration are shown in **Fig. S2**. The Raman signal of sulfate is greatly enhanced by >10 times, which is much higher than previously reported substrates such as Au/Ag nanoparticles array (~2) (Craig et al., 2015) and Klarite (<6) (Fu et al., 2017). It can be seen that as the depth of the gold nanoring cavity increases from 20 nm to 405 nm, the volume of gold nanoring increases; thus, the gaps between nanostructures (holes, pillars and rings) are decreased. The smaller gaps can give rise to larger field enhancement due to the stronger plasmonic coupling between nanostructures (Wei et al., 2008). The reason why the Au nanorings as SERS substrates exhibit high SERS sensitivity originates from the fact that the nanoring structure of the gold. As for a nanoring cavity, more nanostructures, including a hole, a pillar and a ring, are stacked within a unit cell, resulting in additional gaps, edges, and corners (Ho et al., 2014). Moreover, the plasmonic couplings between the nanostructures (a hole, a pillar and a ring) may result in stronger field enhance-

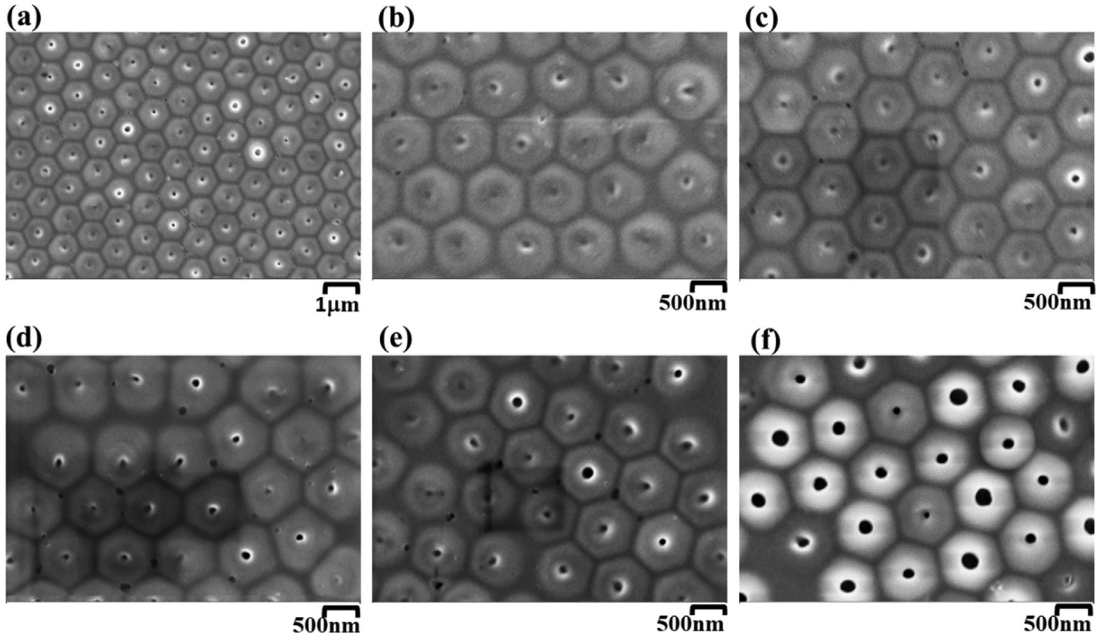

Fig. 1 – (a) Top-view SEM images of the Au nanorings; SEM images of different sputtering duration: (b) 30 sec, (c) 180 sec, (d) 240 sec, (e) 300 sec, (f) 420 sec.

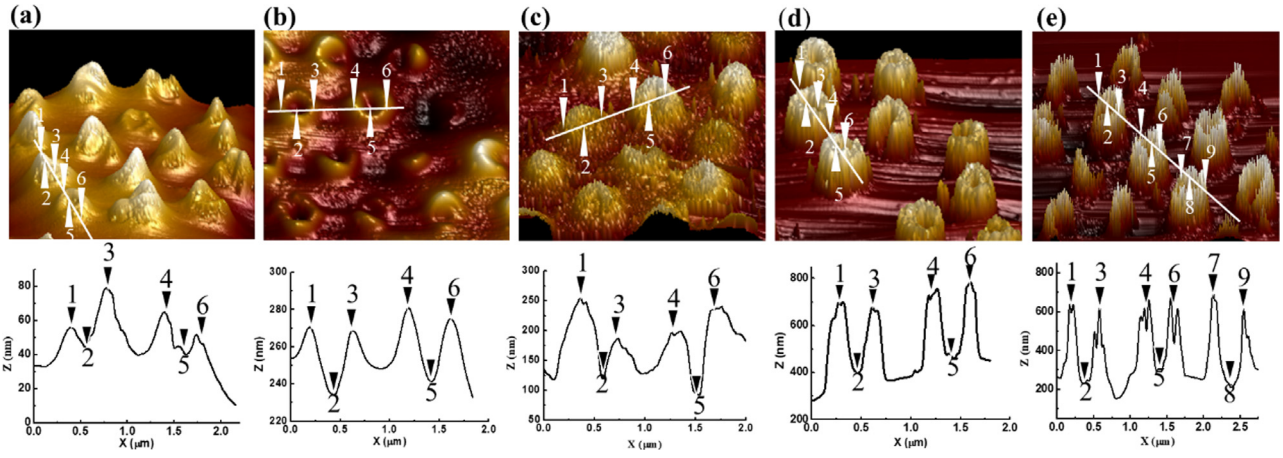

Fig. 2 – AFM topographic and representative line scan images of the Au nanoring submonolayer at different sputtering duration of the fabrication process. (a) 30 sec, (b) 180 sec, (c) 240 sec, (d) 300 sec, and (e) 420 sec. All arrows marked in the topographic images correspond to the arrows in the line scan images.

ment (Félidj et al., 2002). The advantage of nanoring structure compared with nanopillar array is that it has cavities that can better fit in the aerosol particles, and the electric field can be greatly enhanced in these cavities, benefiting Raman signal enhancement. Based on the above results, we found that the Au nanoring arrays have a considerable advantage in SERS performance, which is important for us to distinguish the contribution of SERS signals for atmospheric aerosol particles.

To investigate the reproducibility of the SERS signals based on the Au nanorings as substrates, ten times experimental reflection spectra of $(NH_4)_2SO_4$ aerosols are analyzed in Fig. 3b. The relative standard deviation (RSD) of the intensities of 975 cm^{-1} peaks is 8.1%. This result indicates that the SERS signals based on Au nanoring arrays as substrates are of high reproducibility. Therefore, this experiment confirms that the ordered size and shape distribution of Au nanorings can improve the accuracy for detecting atmospheric aerosol particles.

2.3. *SERS sensitivity of the Au nanoring arrays for atmospheric aerosol particles*

The capability of SERS for detection of composition in individual atmospheric aerosol particle was examined using the Au nanoring arrays substrate. First, the atmospheric aerosol particles were collected on these substrates by using grading particle sampler. For each grade, a total of 10 aerosol particles were randomly selected on Au nanoring arrays substrate for Raman spectrum analysis. The final Raman spectrums of each grade are shown in Fig. 4a after equalization. In the Raman spectrum, it can be found that the components of atmospheric aerosol particles between grading IV and VI are mostly

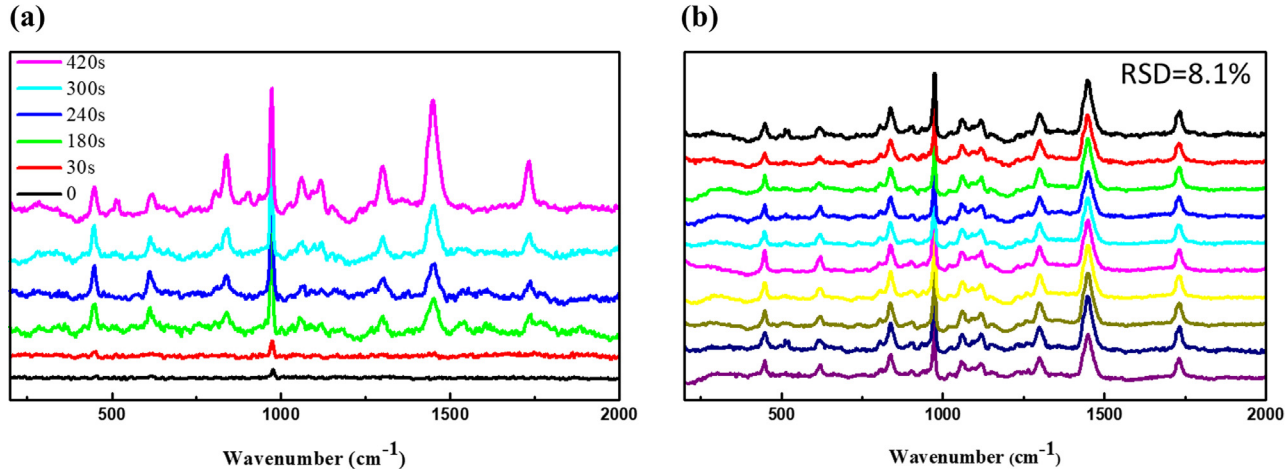

Fig. 3 – SERS spectra of Au Nanorings with different sputtering duration (a); ten times of SERS measurements using identical Au Nanorings as the substrate and the same $(NH_4)_2SO_4$ aerosols as analyte (b).

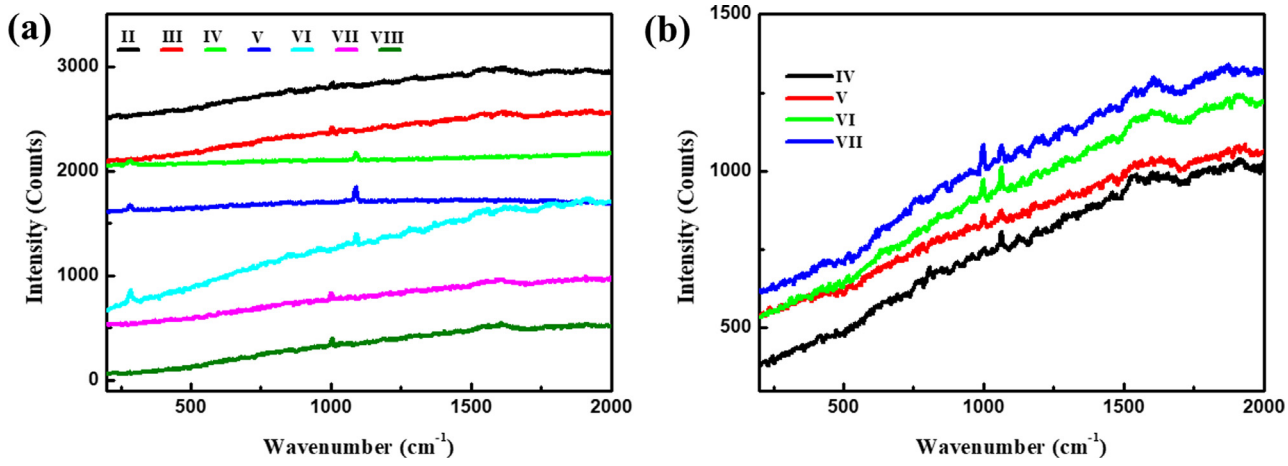

Fig. 4 – SERS spectra of atmospheric aerosol particles collected by grading particle sampler (a); the optimized SERS spectra from grading IV to VII (b).

nitrate (NO_3^-), at 1051 cm^{-1}. Under grading III and up grading VII, the most components are sulfate (SO_4^{2-}), at 975 cm^{-1}. Fig. 4b displays the optimized SERS spectra from grading IV to VII. Comparing the measured SERS signals of curve IV to curve VII in Fig. 4a, the peaks belonging to SO_4^{2-} and NO_3^- can be clearly found. This work demonstrates that the fabricated Au nanoring arrays have promising potential in SERS-based rapid detection of atmospheric aerosol particles.

Fig. 5 exhibits some typical Raman imaging examples of individual atmospheric aerosol particles. The point-by-point Raman scanning acquisition over 2.5 × 2.5 μm^2 area around one individual particle selected by grading particle sampler generates a set of 49 pixel spectra. The careful comparison of each pixel spectrum indicates that typical pixel spectra are characteristic of mixture with several components. Using Raman mapping, the component can be presented visually. It can be seen that these individual particles are probably generated by the agglomeration of sulfate, nitrate, and carbon. Few individual particles composed exclusively of one SO_4^{2-} or NO_3^- species was detected. Most of the particles in atmospheric aerosol are determined by Raman imaging as mixture particle aggregated with SO_4^{2-} and NO_3^-. These results show the po-

Table 1 – Fabrication parameters and dimension of Au nanoring submonolayer structure from AFM.

SAMPLE	Sputtering duration (sec)	Inner diameter(NM)	Shell thickness(NM)	Depth(NM)
(a)	30	366±22	237±11	20±5
(b)	180	433±9	254±28	35.98±9
(c)	240	342±33	317±21	113±14
(d)	300	360±27	299±31	289±14
(e)	420	395±17	269±25	405±33

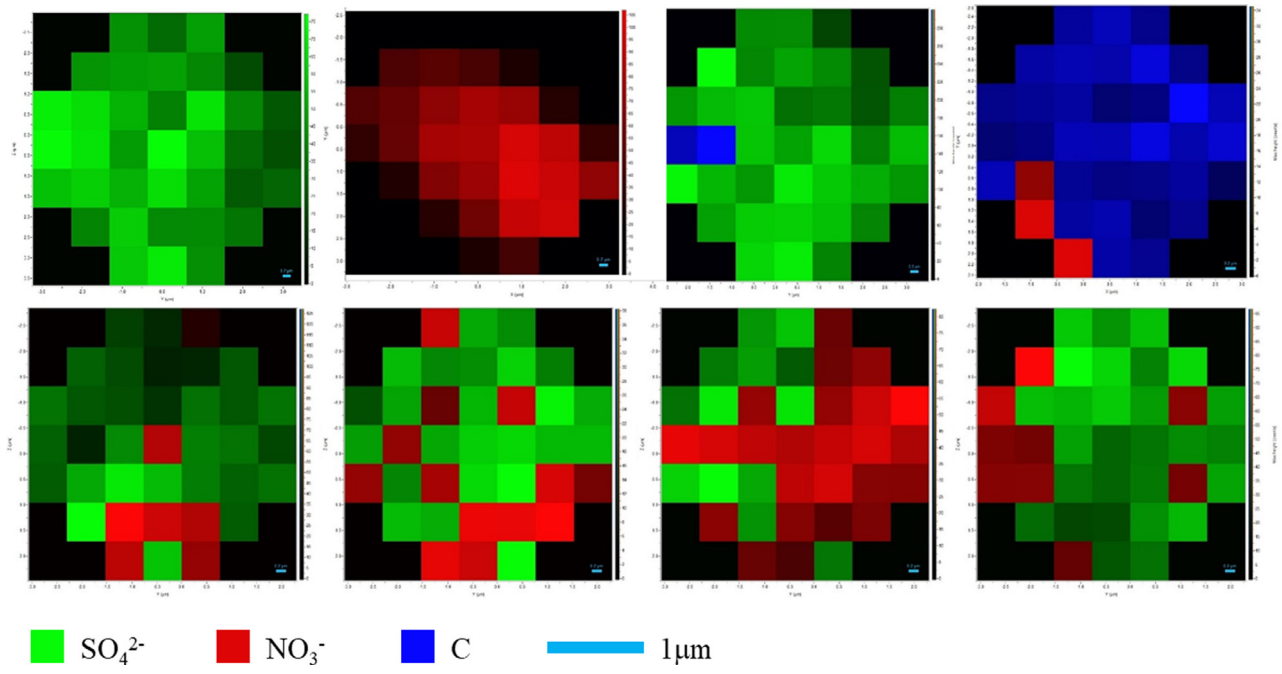

Fig. 5 – Raman images of individual atmospheric aerosol particles.

tential for SERS to enable improved analysis of chemical composition and mixing state of aerosol particles. The ability to detect chemical species in these particles also shows the potential for future SERS work to probe differences in composition at aerosol surfaces due to phase separation, the presence of surfactants, or surface level reactions. Overall, future SERS studies of atmospheric aerosol composition could lead to improved understanding of multiphase atmospheric processing and aerosol impacts on climate and human health.

3. Conclusions

In summary, we demonstrate that ringlike gold nanoparticle arrays used for SERS substrate exhibit tunable plasmon resonances. The volume confined by the nanoring is empty and therefore have a considerable advantage in SERS applications for individual atmospheric aerosols particle detection. The experimentally observed SERS signals of these structures used for detection of laboratory-generated and ambient aerosol particles is well described. Using Raman mapping, the distribution information on chemical components of the individual aerosol particles, which might not be possible with the methods based on mass spectrometry or chromatography can be more readily and quickly. This work provides an efficient SERS substrate that can be easily fabricated in large scale for chemical component and mixing state study of individual aerosol particles, which are of great importance if one wants to know the climate and health effect of the particles.

Acknowledgments

This work was supported by the National Natural Science Foundation of China (No. 21976030 and No. 21677037), and the Natural Science Foundation of Shanghai (No. 19ZR1471200 and No. 17ZR1440200).

Appendix A Supplementary data

Supplementary material associated with this article can be found, in the online version, at doi:10.1016/j.jes.2020.07.003.

REFERENCES

Alharbi, O., Xu, Y., Goodacre, R., 2014. Simultaneous multiplexed quantification of nicotine and its metabolites using surface enhanced Raman scattering. Analyst 139, 4820.

Andreae, M.O., Rosenfeld, D., 2008. Aerosol-cloud-precipitation interactions. Part 1. The nature and sources of cloud-active aerosols. Earth Sci. Rev. 89, 13.

Aubriet, F., Carre, V., 2010. Potential of laser mass spectrometry for the analysis of environmental dust particles–a review. Anal. Chim. Acta 659, 34.

Ault, A.P., Axson, J.L., 2017. Atmospheric aerosol chemistry: spectroscopic and microscopic advances. Anal. Chem. 89, 430.

Ault, A.P., Moffet, R.C., Baltrusaitis, J., Collins, D.B., Ruppel, M.J., Cuadra-Rodriguez, L.A., et al., 2013. Size-dependent changes in sea spray aerosol composition and properties with different seawater conditions. Environ. Sci. Technol. 47, 5603.

Baustian, K.J., Cziczo, D.J., Wise, M.E., Pratt, K.A., Kulkarni, G., Hallar, A.G., et al., 2012. Importance of aerosol composition, mixing state, and morphology for heterogeneous ice nucleation: a combined field and laboratory approach. J. Geophys. Res. Atmos. 117, D06217.

Canagaratna, M.R., Jayne, J.T., Jimenez, J.L., Allan, J.D., Alfarra, M.R., Zhang, Q., et al., 2007. Chemical and microphysical characterization of ambient aerosols with the aerodyne aerosol mass spectrometer. Mass Spectrom. Rev. 26, 185.

Cialla, D., Marz, A., Bohme, R., Theil, F., Weber, K., Schmitt, M., et al., 2012. Surface-enhanced Raman spectroscopy (SERS): progress and trends. Anal. Bioanal. Chem. 403, 27.

Clauson, S.L., Sylvia, J.M., Arcury, T.A., Summers, P., Spencer, K.M., 2015. Detection of pesticides and metabolites using surface-enhanced Raman spectroscopy (SERS): acephate. Appl. Spectrosc. 69, 785.

Craig, R.L., Bondy, A.L., Ault, A.P., 2015. Surface enhanced Raman spectroscopy enables observations of previously undetectable secondary organic aerosol components at the individual particle level. Anal. Chem. 87, 7510.

Dong, J.L., Li, X.H., Zhao, L.J., Xiao, H.S., Wang, F., Guo, X., et al., 2007. Raman observation of the interactions between NH_4^+, SO_4^{2-}, and H_2O in supersaturated $(NH_4)_2SO_4$ droplets. J. Phys. Chem. B 111, 12170.

Dong, X., Ohnoutek, L., Yang, Y., Feng, Y., Wang, T., Tahir, M.A., et al., 2019. Cu/Ag sphere segment void array as efficient surface enhanced Raman spectroscopy substrate for detecting individual atmospheric aerosol. Anal. Chem. 91, 13647.

Eberhardt, K., Stiebing, C., Matthaus, C., Schmitt, M., Popp, J., 2015. Advantages and limitations of Raman spectroscopy for molecular diagnostics: an update. Expert Rev. Mol. Diagn. 15, 773.
Elmes, M., Gasparon, M., 2017. Sampling and single particle analysis for the chemical characterisation of fine atmospheric particulates: a review. J. Environ. Manag. 202, 137.
Félidj, N., Aubard, J., Lévi, G., Krenn, J.R., Salerno, M., Schider, G., et al., 2002. Controlling the optical response of regular arrays of gold particles for surface-enhanced Raman scattering. Phys. Rev. B 65, 075419.
Fierce, L., Bond, T.C., Bauer, S.E., Mena, F., Riemer, N., 2016. Black carbon absorption at the global scale is affected by particle-scale diversity in composition. Nat. Commun. 7, 12361.
Fu, Y., Kuppe, C., Valev, V.K., Fu, H., Zhang, L., Chen, J., 2017. Surface-enhanced Raman spectroscopy: a facile and rapid method for the chemical component study of individual atmospheric aerosol. Environ. Sci. Technol. 51, 6260.
Gilardoni, S., Massoli, P., Paglione, M., Giulianelli, L., Carbone, C., Rinaldi, M., et al., 2016. Direct observation of aqueous secondary organic aerosol from biomass-burning emissions. Proc. Natl. Acad. Sci. U. S. A. 113, 10013.
Hallquist, M., Wenger, J.C., Baltensperger, U., Rudich, Y., Simpson, D., Claeys, M., et al., 2009. The formation, properties and impact of secondary organic aerosol: current and emerging issues. Atmos. Chem. Phys. 9, 5155.
Hatch, L.E., Creamean, J.M., Ault, A.P., Surratt, J.D., Chan, M.N., Seinfeld, J.H., et al., 2011. Measurements of isoprene-derived organosulfates in ambient aerosols by aerosol time-of-flight mass spectrometry - part 1: single particle atmospheric observations in Atlanta. Environ. Sci. Technol. 45, 5105.
Ho, C.C., Zhao, K., Lee, T.Y., 2014. Quasi-3D gold nanoring cavity arrays with high-density hot-spots for SERS applications via nanosphere lithography. Nanoscale 6, 8606.
Jordanov, N., Zellner, R., 2006. Investigations of the hygroscopic properties of ammonium sulfate and mixed ammonium sulfate and glutaric acid micro droplets by means of optical levitation and Raman spectroscopy. Phys. Chem. Chem. Phys. 8, 2759.
Li, L., Huang, Z.X., Dong, J.G., Li, M., Gao, W., Nian, H.Q., et al., 2011. Real time bipolar time-of-flight mass spectrometer for analyzing single aerosol particles. Int. J. Mass Spectrom. 303, 118.
Noble, C.A., Prather, K.A., 1996. Real-time measurement of correlated size and composition profiles of individual atmospheric aerosol particles. Environ. Sci. Technol. 30, 2667.
Offroy, M., Moreau, M., Sobanska, S., Milanfar, P., Duponchel, L., 2015. Pushing back the limits of Raman imaging by coupling super-resolution and chemometrics for aerosols characterization. Sci. Rep. 5, 12303.
Parshintsev, J., Hyotylainen, T., 2015. Methods for characterization of organic compounds in atmospheric aerosol particles. Anal. Bioanal. Chem. 407, 5877.
Perez-Fernandez, V., Mainero Rocca, L., Tomai, P., Fanali, S., Gentili, A., 2017. Recent advancements and future trends in environmental analysis: sample preparation, liquid chromatography and mass spectrometry. Anal. Chim. Acta 983, 9.
Perrino, C., Marcovecchio, F., 2016. A new method for assessing the contribution of primary biological atmospheric particles to the mass concentration of the atmospheric aerosol. Environ. Int. 87, 108.
Poschl, U., 2005. Atmospheric aerosols: composition, transformation, climate and health effects. Angew. Chem. Int. Ed. Engl. 44, 7520.
Riemer, N., West, M., 2013. Quantifying aerosol mixing state with entropy and diversity measures. Atmos. Chem. Phys. 13, 11423.
Roth, A., Schneider, J., Klimach, T., Mertes, S., van Pinxteren, D., Herrmann, H., et al., 2016. Aerosol properties, source identification, and cloud processing in orographic clouds measured by single particle mass spectrometry on a central European mountain site during HCCT-2010. Atmos. Chem. Phys. 16, 505.
Schlucker, S., 2014. Surface-enhanced Raman spectroscopy: concepts and chemical applications. Angew. Chem. Int. Ed. Engl. 53, 4756.
Sun, Z., Duan, F., He, K., Du, J., Yang, L., Li, H., et al., 2019. Physicochemical analysis of individual atmospheric fine particles based on effective surface-enhanced Raman spectroscopy. J. Environ. Sci. (China) 75, 388.
Teich, M., van Pinxteren, D., Kecorius, S., Wang, Z., Herrmann, H., 2016. First quantification of imidazoles in ambient aerosol particles: potential photosensitizers, brown carbon constituents, and hazardous components. Environ. Sci. Technol. 50, 1166.
Virtanen, A., Joutsensaari, J., Koop, T., Kannosto, J., Yli-Pirila, P., Leskinen, J., et al., 2010. An amorphous solid state of biogenic secondary organic aerosol particles. Nature 467, 824.
Wei, H., Hakanson, U., Yang, Z., Hook, F., Xu, H., 2008. Individual nanometer hole-particle pairs for surface-enhanced Raman scattering. Small 4, 1296.
Xu, W., Croteau, P., Williams, L., Canagaratna, M., Onasch, T., Cross, E., et al., 2017. Laboratory characterization of an aerosol chemical speciation monitor with PM2.5 measurement capability. Aerosol Sci. Tech. 51, 69.
Yang, J., Ma, S., Gao, B., Li, X., Zhang, Y., Cai, J., et al., 2017. Single particle mass spectral signatures from vehicle exhaust particles and the source apportionment of on-line PM2.5 by single particle aerosol mass spectrometry. Sci. Total. Environ. 593-594, 310.
Zaveri, R.A., Shilling, J.E., Zelenyuk, A., Liu, J., Bell, D.M., D'Ambro, E.L., et al., 2018. Growth kinetics and size distribution dynamics of viscous secondary organic aerosol. Environ. Sci. Technol. 52, 1191.
Zhang, Q., Jimenez, J.L., Canagaratna, M.R., Ulbrich, I.M., Ng, N.L., Worsnop, D.R., et al., 2011. Understanding atmospheric organic aerosols via factor analysis of aerosol mass spectrometry: a review. Anal. Bioanal. Chem. 401, 3045.